Research Article | Vol. 28, No. 19 / 14 September 2020 / Optics Express 27547
Optics EXPRESS

Multipole interplay controls optical forces and ultra-directional scattering

ANDREI KISELEV,[1,2] KARIM ACHOURI,[1] AND OLIVIER J. F. MARTIN[1,3]

[1] *Nanophotonics and Metrology Laboratory, Swiss Federal Institute of Technology Lausanne (EPFL), 1015 Lausanne, Switzerland*
[2] *andrei.kiselev@epfl.ch*
[3] *olivier.martin@epfl.ch*

Abstract: We analyze the superposition of Cartesian multipoles to reveal the mechanisms underlying the origin of optical forces. We show that a multipolar decomposition approach significantly simplifies the analysis of this problem and leads to a very intuitive explanation of optical forces based on the interference between multipoles. We provide an in-depth analysis of the radiation coming from the object, starting from low-order multipole interactions up to quadrupolar terms. Interestingly, by varying the phase difference between multipoles, the optical force as well as the total radiation directivity can be well controlled. The theory developed in this paper may also serve as a reference for ultra-directional light steering applications.

1. Introduction

Optical trapping – the ability to manipulate objects from the nano and micro worlds with light – has been instrumental in developing of many areas of physics, biology and material sciences [1–11]. Stable trapping can be successfully performed in free space for objects with dimensions larger or comparable to the trapping laser wavelength [12–15] and even beat the Abbe's diffraction limit by localizing particles within areas as small as only a few tens of nanometers with the aid of nanotweezers [16–21].

The optical force acting on particles can be separated into gradient, absorption and scattering components [13,22]. The gradient component drags a particle towards the laser focus, thus enabling stable trapping [1,13]. The absorption force, caused by the intrinsic loss of the material, and the scattering force are very rich in terms of the mechanical actions they can produce, such as propelling, pulling and rotating particles [23–25].

The optical force may be analyzed by integrating Maxwell's stress tensor over a virtual sphere enclosing the scatterer [26]. Since Maxwell's stress tensor is expressed in terms of the incident and scattered electric and magnetic fields, it follows that the total optical force has terms consisting of the products of these different fields. Specifically, the terms resulting from the interactions of incident and scattered fields are usually referred to as the incident-scattered interactions, while those resulting from the products of scattered and scattered fields are commonly referred to as the scattered-scattered interactions [27,28]. Note that there is no interaction of the incident fields with themselves. The incident-scattered interactions are associated with the scattering and absorption in the material, while the scattered-scattered interactions are attributed to scattering from the object [29]. To gain insights into the origin of both forces, it is useful to analyze them in the framework of a multipole decomposition, by inserting different multipole contributions into Maxwell's stress tensor [26,27,30–33].

The scattering-scattering interactions result in a force associated with the radiation asymmetry coming from the object. For objects radiating as only one single multipole, the scattering force always vanishes due to the symmetrical radiation pattern of any isolated multipole [33]. The situation changes when the object radiates as the sum of several multipoles. Indeed, in

#400387 https://doi.org/10.1364/OE.400387
Journal © 2020 Received 9 Jul 2020; revised 21 Aug 2020; accepted 24 Aug 2020; published 2 Sep 2020

Optics EXPRESS

this circumstance they can produce asymmetric radiation patterns, leading to a non-negligible optical force. In the case of resonating scatterers, the force may even reach very high values when driven at the resonance [34–37]. In some cases, the asymmetric radiation pattern may be forward-directed so that it can even overcome the pushing stream of incident photons, thus resulting in an overall pulling force [38–45]. Moreover, the radiation pattern asymmetry can also result in an unexpected transversal force in a crossed beams illumination configuration due to a nonnegligible transversal component of the real part of the Poynting vector [46–50]. Additionally, it was shown that the imaginary part of the Poynting vector can also contribute to the light-matter momentum exchange [51], to enhance the sorting and size selectivity of optical tweezers [52] or to rotate a particle illuminated by cylindrical vector beams without incident spin or orbital momenta [53].

The incident-scattering interactions can also be described in terms of interactions between multipoles. However, since it is common practice to define the incident field exciting the scatterer as a simple plane wave, it is thus easier to resort to Taylor expansion rather than multipole decomposition to approximate it [39,51]. Alternatively, a vector spherical harmonic representation may be used to describe incident and scattered waves [27,54]. Please note that care should be taken to accurately estimate the multipolar response of a structure [55,56].

Tedious calculations are required to obtain even simple expressions for the force appearing due to different multipole combinations [27,39,51,54]. These expressions reveal how the optical force depends on the relative magnitude and the phase difference between interacting multipoles. Having all the equations at hand [27,39,51], the reader might still deliberate about the origin of the force appearing due to multipoles interactions for different relative amplitudes and phases. This leads to the first aim of this paper: providing the reader with a comprehensive visual analysis of various interactions between multipoles and their resulting optical forces. The second aim is to equip the nanophotonics and radiofrequency communities with a visual explanation of radiation directivity for different multipoles interactions. This analysis has bearing on important problems related to light steering in systems such as high refractive index materials, core-shell nanoparticles, metamaterials, chiral materials and Huygens sources [39,57–71]. In addition, the knowledge about the intensity distributions for higher order multipoles interactions is of particular importance in the context of ultra-directional scattering [72–75]. This work is also relevant for the second harmonic generation community, since the interaction between multipoles both at the fundamental and at the second harmonic frequencies governs the second harmonic response [62,76–84].

This paper is organized as follows: in the methods section we analyze the different multipoles interaction terms in Maxwell's stress tensor. We show that the knowledge of the total intensity distribution is not required for computing the optical force resulting from the interaction of the multipole pairs. Instead, the interference effects between those multipoles appear to be responsible for the emergence of the force. In the results section, we present the interference and intensity distributions for all possible multipole interactions up to the quadrupolar-quadrupolar terms, demonstrating a strong shaping of the radiation directivity upon variation of the constituting multipoles' relative intensity and phase.

2. Methods

In this section, we discuss the contributions of the different terms in Maxwell's stress tensor. We show that a multipolar decomposition of the fields significantly simplifies the corresponding equations and leads to an intuitive analysis of the force in the framework of the interference term.

Optics EXPRESS

2.1. Computation of the optical force resulting from two interacting multipoles

The optical force acting on an arbitrary object can be found by integrating the electric (**E**) and magnetic (**H**) fields on a virtual sphere Ω with outward normal **n** enclosing that object [26]:

$$\langle \mathbf{F} \rangle = \int_{\Omega} \frac{1}{2} \mathrm{Re} \left[\varepsilon_0 \varepsilon_r \mathbf{E}(\mathbf{E}^* \cdot \mathbf{n}) + \mu_0 \mu_r \mathbf{H}(\mathbf{H}^* \cdot \mathbf{n}) - \frac{1}{2}(\varepsilon_0 \varepsilon_r \mathbf{E} \cdot \mathbf{E}^*)\mathbf{n} - \frac{1}{2}(\mu_0 \mu_r \mathbf{H} \cdot \mathbf{H}^*)\mathbf{n} \right] dS, \quad (1)$$

where ε_r and μ_r are the relative permittivity and permeability of the surrounding medium and dS is a surface element on the virtual sphere. The double bracket represents a time-averaging operation. For simplicity, we hereafter assume vacuum as a background medium with $\varepsilon_r = \mu_r = 1$. To analyze the scattering from a subwavelength particle and subsequently deduce the resulting optical force, we consider that its electromagnetic response may be expressed as a superposition of Cartesian multipoles [33,39]. The optical force is therefore determined from the contributions of a series of interfering multipoles pairs [39]. To this end, let us consider two arbitrary Cartesian multipoles oscillating at the same frequency ω and placed at the center of the virtual sphere Ω. The first multipole radiates an electromagnetic field $(\mathbf{E}_1, \mathbf{H}_1)$, while the second radiates an electromagnetic field $(\mathbf{E}_2, \mathbf{H}_2)$. Furthermore, for a virtual sphere Ω with diameter d much larger than the wavelength, the outgoing electromagnetic waves of these multipoles become transverse in the far-field, implying that on the virtual sphere,

$$\mathbf{E}_i \cdot \mathbf{n} = \mathbf{H}_i \cdot \mathbf{n} = 0, \qquad i = 1, 2. \quad (2)$$

Thus, Eq. (1) can be simplified to

$$\langle \mathbf{F} \rangle = -\int_{\Omega} \frac{1}{2} \mathrm{Re} \left[\frac{1}{2}(\varepsilon_0 \mathbf{E} \cdot \mathbf{E}^*)\mathbf{n} + \frac{1}{2}(\mu_0 \mathbf{H} \cdot \mathbf{H}^*)\mathbf{n} \right] dS. \quad (3)$$

In the far-field, the electric and magnetic components of a spherical wave are related through the impedance of vacuum [85],

$$Z_0 = \sqrt{\frac{\mu_0}{\varepsilon_0}} = \frac{|E|}{|H|}, \quad (4)$$

which reduces Eq. (3) to

$$\langle \mathbf{F} \rangle = -\int_{\Omega} \frac{1}{2} \mathrm{Re}[(\varepsilon_0 \mathbf{E} \cdot \mathbf{E}^*)\mathbf{n}] dS. \quad (5)$$

We may now express the force resulting from the interference of the two radiating multipoles by writing the total electric field as a sum of their contributions:

$$\mathbf{E} = \mathbf{E}_1 + \mathbf{E}_2. \quad (6)$$

Inserting Eq. (6) into Eq. (5), leads to

$$\begin{aligned} \langle \mathbf{F} \rangle &= -\int_{\Omega} \mathrm{Re}\left[\tfrac{1}{2}(\varepsilon_0 \mathbf{E} \cdot \mathbf{E}^*)\mathbf{n}\right] dS = \\ &-\int_{\Omega} \mathrm{Re}\left[\tfrac{1}{2}(\varepsilon_0[\mathbf{E}_1 \cdot \mathbf{E}_1{}^* + \mathbf{E}_2 \cdot \mathbf{E}_2{}^* + \mathbf{E}_1 \cdot \mathbf{E}_2{}^* + \mathbf{E}_2 \cdot \mathbf{E}_1{}^*])\mathbf{n}\right] dS = \\ &-\tfrac{1}{c_0}\int_{\Omega} \left[\left[I_1 + I_2 + c_0 \mathrm{Re}\tfrac{1}{2}(\varepsilon_0[\mathbf{E}_1 \cdot \mathbf{E}_2{}^* + \mathbf{E}_2 \cdot \mathbf{E}_1{}^*])\right]\mathbf{n}\right] dS = \\ &-\tfrac{1}{c_0}\int_{\Omega} [[I_1 + I_2 + c_0 \mathrm{Re}(\varepsilon_0[\mathbf{E}_1 \cdot \mathbf{E}_2{}^*])]\mathbf{n}] dS, \end{aligned} \quad (7)$$

where

$$I_i = \frac{c_0 \varepsilon_0}{2} \mathbf{E}_i \cdot \mathbf{E}_i{}^*, \quad (8)$$

is the intensity of the waves with c_0 being the speed of light in vacuum. Due to the fact that single multipoles have a symmetric intensity distribution [33], the first two integrals in Eq. (7)

Optics EXPRESS

vanish. It follows that the equation for the force becomes

$$\langle \mathbf{F} \rangle = -\int_{\Omega} [[\mathrm{Re}(\varepsilon_0[\mathbf{E}_1 \cdot \mathbf{E}_2{}^*])]\mathbf{n}]dS. \tag{9}$$

This equation reveals that the interference between two multipoles directly determines the optical force.

2.2. Link between optical force and Cartesian multipoles

We follow here the derivation provided by Chen et al. and start by recalling their main results for completeness [39]. If the object is small compared to the wavelength, the radiation produced in the far-field may be approximated (up to quadrupolar term) by the radiating electric dipole moment $\mathbf{p}(t)$, electric quadrupole moment tensor $\overleftrightarrow{\mathbf{q}}^e(t)$, magnetic dipole moment $\mathbf{m}(t)$ and magnetic quadrupole moment tensor $\overleftrightarrow{\mathbf{q}}^m(t)$ [33,39].

For a monochromatic wave oscillating at frequency ω, the oscillating multipoles can be represented by their complex-valued time-harmonic counterparts $\mathbf{p}$, $\mathbf{m}$, $\overleftrightarrow{\mathbf{q}}^e$, $\overleftrightarrow{\mathbf{q}}^m$ linked with the original multipoles by the following equations $\mathbf{p}(t) = \mathrm{Re}[e^{-i\omega t}\mathbf{p}]$, $\overleftrightarrow{\mathbf{q}}^e(t) = \mathrm{Re}[e^{-i\omega t}\overleftrightarrow{\mathbf{q}}^e]$, $\mathbf{m}(t) = \mathrm{Re}[e^{-i\omega t}\mathbf{m}]$ and $\overleftrightarrow{\mathbf{q}}^m(t) = \mathrm{Re}[e^{-i\omega t}\overleftrightarrow{\mathbf{q}}^m]$. The electric field distribution in the far-field in the time-harmonic representation and at a point with coordinate R can then be written as [33,39]

$$\mathbf{E} = \frac{k^2}{4\pi\varepsilon_0}\frac{e^{ikR-i\omega t}}{R}\left[\mathbf{n}\times(\mathbf{p}\times\mathbf{n}) + \frac{1}{c_0}(\mathbf{m}\times\mathbf{n}) + \frac{ik}{2}\mathbf{n}\times\left[\mathbf{n}\times\left(\overleftrightarrow{\mathbf{q}}^e\cdot\mathbf{n}\right)\right] + \frac{ik}{2c_0}\mathbf{n}\times\left(\overleftrightarrow{\mathbf{q}}^m\cdot\mathbf{n}\right)\right], \tag{10}$$

here k is a wave vector, $\mathbf{n}$ is a vector normal to the sphere Ω.

Let us analyze the symmetry properties of the electric field produced by the different multipoles in Eq. (10). The electric field can be classified as symmetric if it does not change in the case of a sign substitution, i.e., $\mathbf{n} \to -\mathbf{n}$, which is the case for an electric dipole and a magnetic quadrupole. The electric field is considered antisymmetric if its sign changes, which is the case for a magnetic dipole and an electric quadrupole. The combination of two multipoles with different symmetry properties can lead to an asymmetric radiation pattern, which, according to Eq. (7), leads to a net optical force. Consequently, interactions leading to an asymmetric radiation pattern are possible only for the following pairs of multipoles: ($\mathbf{p}$ and $\mathbf{m}$), ($\mathbf{p}$ and $\overleftrightarrow{\mathbf{q}}^e$), ($\mathbf{m}$ and $\overleftrightarrow{\mathbf{q}}^m$), ($\overleftrightarrow{\mathbf{q}}^e$ and $\overleftrightarrow{\mathbf{q}}^m$), while all other combinations lead to symmetric radiation patterns. From Eq. (7), it is apparent that this leads to a nonzero integral of the intensity over the sphere Ω and thus results in a nonzero net optical force.

Since the electric potential satisfies the Laplace equation, the six components of the quadrupolar tensor are not independent, which makes the tensors overdetermined [86,87]. For convenience, the quadrupolar tensor is usually redefined to make it symmetric and traceless, which naturally reduces the number of components to five. This also helps, for example, to circumvent the problem of zero potential for spherical capacitors, which have a zero net charge [88–90]:

$$Q^e_{ij} = q^e_{ij} - \frac{1}{3}q^e_{ss}\delta_{ij}, \tag{11}$$

$$Q^m_{ij} = \frac{1}{2}(q^m_{ij} + q^m_{ji}). \tag{12}$$

here $q^e_{ss} = q^e_{xx} + q^e_{yy} + q^e_{zz}$. We would like to mention that a Cartesian toroidal dipole usually appears at this step as a result of quadrupoles symmetrization. However, note that the far-field distribution of a toroidal dipole exactly matches the far-field produced by an electric dipole and only differs by a $\pi/2$ relative phase shift [87]. Therefore, we will not discuss separately the cases

Optics EXPRESS

of toroidal and dipolar multipoles in the forthcoming developments. For more information, one may refer to the very detailed analysis of the forces resulting from the interactions with toroidal multipoles provided in [91].

The optical force along the i-axis $\langle \mathbf{F} \rangle_i$ in a Cartesian coordinate system can then be found by inserting the electric field produced by Cartesian multipoles [39]. Using the traceless multipoles notation, Eqs. (11) and (12), the equation for the force then takes the following form

$$\begin{aligned} \langle \mathbf{F} \rangle_i = &-\frac{k^4}{12\pi\varepsilon_0 c_0}\mathrm{Re}\left[\sum_{j,k}\varepsilon_{ijk}p_j m_k^*\right] - \frac{k^5}{40\pi\varepsilon_0}\mathrm{Im}[Q^e_{ij}p_j^*] \\ &-\frac{k^5}{40\pi\varepsilon_0 c_0^2}\mathrm{Im}[Q^m_{ij}m_j^*] - \frac{k^6}{240\pi\varepsilon_0 c_0}\mathrm{Re}\left[\sum_{l,j,k}\varepsilon_{ijk}Q^e_{lj}Q^{m*}_{lk}\right], \end{aligned} \tag{13}$$

where ε_{ijk} is the Levi-Civita tensor [92].

The understanding of this formula is at the core of this paper. For the purpose of visualization, we hereafter consider only the force appearing along the z-axis of a Cartesian coordinate system. From Eq. (13), the force along the z-axis can be expressed as

$$\begin{aligned} \langle \mathbf{F} \rangle_z = &-\frac{k^4}{12\pi\varepsilon_0 c_0}\mathrm{Re}[p_x m_y^* - p_y m_x^*] \\ &-\frac{k^5}{40\pi\varepsilon_0}\mathrm{Im}[Q^e_{zx}p_x^* + Q^e_{zy}p_y^* + Q^e_{zz}p_z^*] \\ &-\frac{k^5}{40\pi\varepsilon_0 c_0^2}\mathrm{Im}[Q^m_{zx}m_x^* + Q^m_{zy}m_y^* + Q^m_{zz}m_z^*] \\ &-\frac{k^6}{240\pi\varepsilon_0 c_0}\mathrm{Re}\left[\begin{array}{l} Q^e_{xx}Q^{m*}_{xy} - Q^e_{yy}Q^{m*}_{yx} + Q^e_{yx}Q^{m*}_{yy} + \\ -Q^e_{xy}Q^{m*}_{xx} + Q^e_{zx}Q^{m*}_{zy} - Q^e_{zy}Q^{m*}_{zx} \end{array}\right]. \end{aligned} \tag{14}$$

Only the interference terms between these multipoles lead to a force in this specific direction. The origin of the optical force for all these combinations will be discussed in the following sections.

As a supplement to this paper, we provide an open access data containing the code used to simulate the interference and find the optical force resulting from the interaction between an electric dipole p_x with a magnetic dipole m_y [93].

3. Results

We now explore the different terms in Eq. (14) and study some typical combinations of multipole pairs leading to interesting optical forces, taking also in consideration the phase between both multipoles, as well as their relative magnitude.

3.1. Dipole–dipole interaction

Let us first consider the optical force resulting from the interactions between two dipoles. From Eq. (14), it stands out that in this case the force along the z-axis appears due to the interactions of two pairs of electric and magnetic dipoles: p_x with m_y or p_y with m_x. Consider the first pair for which each *individual* radiating multipole has a centrally symmetric radiation intensity distribution and thus does not produce any force. When combined together, they produce an asymmetric intensity pattern giving rise to a force acting on them according to Eq. (7).

The intensity distributions for these electric and magnetic dipoles are shown in Fig. 1. We have normalized p_x and m_y such that the maximum of their respective radiated power is equal. In Fig. 1, the colors represent the intensity magnitude: white for zero values and red for maximum. From these figures, we see that the intensity is simultaneously strong along the $\pm z$-directions for both dipoles. Consequently, we expect to obtain, for a certain phase difference, a strong

Optics EXPRESS

interference between them along the z-axis. As shown in Eq. (7), the total intensity I_{tot} can be obtained as a sum of three terms:

$$I_{tot} = I_1 + I_2 + c_0 \mathrm{Re}(\varepsilon_0[\mathbf{E}_1 \cdot \mathbf{E}_2{}^*]). \tag{15}$$

The first two terms in Eq. (15), corresponding to the intensity of the individual dipoles, are plotted in Fig. 1(a) and 1(b). The third term, representing the interactions of the two multipoles, is plotted in Fig. 1(c), where the blue colors correspond to negative values. The total intensity distribution, I_{tot}, is shown in Fig. 1(e). The dipoles oscillate at the frequency ω with the phase difference $\Delta\phi$ according to:

$$\mathbf{p} = \mathbf{e}_x p_x e^{-i\omega t}, \tag{16}$$

$$\mathbf{m} = \mathbf{e}_y m_y e^{-i\omega t + i\Delta\phi}. \tag{17}$$

Here $\mathbf{e}_x$ and $\mathbf{e}_y$ are Cartesian unit vectors, p_x and m_y are the amplitudes of the electric and magnetic dipoles.

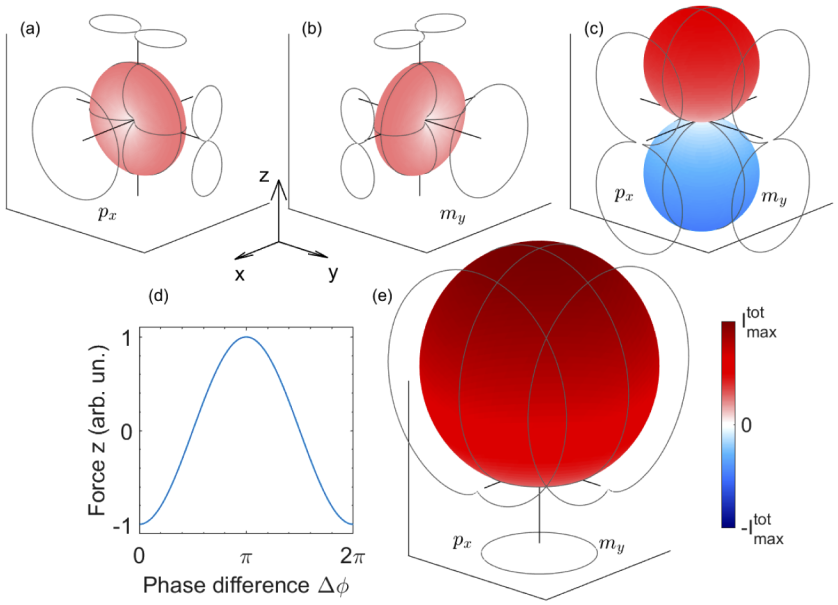

Fig. 1. Origin of the optical force resulting from the superposition of an electric dipole p_x with a magnetic dipole m_y, as a function of their relative phase difference $\Delta\phi$. (a) Radiation pattern for the electric dipole. (b) Radiation pattern for the magnetic dipole. (c) Interference pattern for $\Delta\phi = 0$. (d) Normalized force dependency on the relative phase difference between both multipoles. (e) Total intensity distribution due to the sum of both multipoles. All patterns are normalized to the maximum intensity in panel (e). (Visualization 1) Intensity distribution for different values of the relative phase difference.

For $\Delta\phi = 0$ the total intensity lobe is prominent in the $+z$-direction, Fig. 1(e). Such situation, in which radiation is suppressed in one direction can be realized with the Kerker effect [52,68,94–99]. Intuitively, assuming that each scattered photon carries some momentum, one may expect a negative force acting on the particle by conservation of momentum. This is confirmed by evaluating Eq. (7), as indicated in Fig. 1(d). Interestingly, the directivity of the intensity lobe can be adjusted by changing the phase difference $\Delta\phi$, which is illustrated in Visualization 1. Consequently, the force also changes its magnitude and direction according to Eq. (7). The normalized force changes as a cosines function of the phase difference, in agreement with Eq. (14). This example provides an insightful and intuitive understanding of the total force.

Optics EXPRESS

Next, we show how the total intensity depends on the amplitude ratio between both multipoles. We have chosen the phase difference between both multipoles as $\Delta\phi = \pi$ (the force is positive in that case, as seen from Fig. 1(d)). Then, we vary the amplitude ratio $A = \sqrt{I^{p_x}_{max}/I^{m_y}_{max}}$ from 0 to 1.2. The resulting intensity distribution for both multipoles, the corresponding interference term, force and total intensity are presented in Visualization 2. From Visualization 1 and Visualization 2, it is apparent that the total intensity term presented in panel (e) strongly depends on the amplitude ratio and the phase. Interestingly, the interference term in panel (c) is the one that conserves its shape and is merely scaled, depending on the amplitude or the phase differences, as follows from Eq. (9). The interference term presented in panel (c) can thus serve as a universal parameter suitable for the analysis of experiments with arbitrary phases and amplitudes.

A separate discussion of the interaction between p_y and m_x is not required because their corresponding radiation patterns are similar to those previously discussed. Indeed, the radiation pattern of p_y can be obtained by rotating the radiation pattern of p_x by $\pi/2$ around the z-axis. Similarly, the radiation pattern of m_x can be obtained by rotating the radiation pattern of m_y by the same angle. Consequently, the interference and total intensity patterns for p_y and m_x can be obtained by rotating the data presented in Fig. 1. We will use this approach to expedite the discussion for several interaction terms from Eq. (14), for which an additional visualization does not provide further information.

3.2. Dipole–quadrupole interaction

In this section, we analyze the dipolar-quadrupolar interaction terms in Eq. (14). The corresponding distribution for the p_x and Q^e_{zx} interaction is presented in Fig. 2 for the phase difference

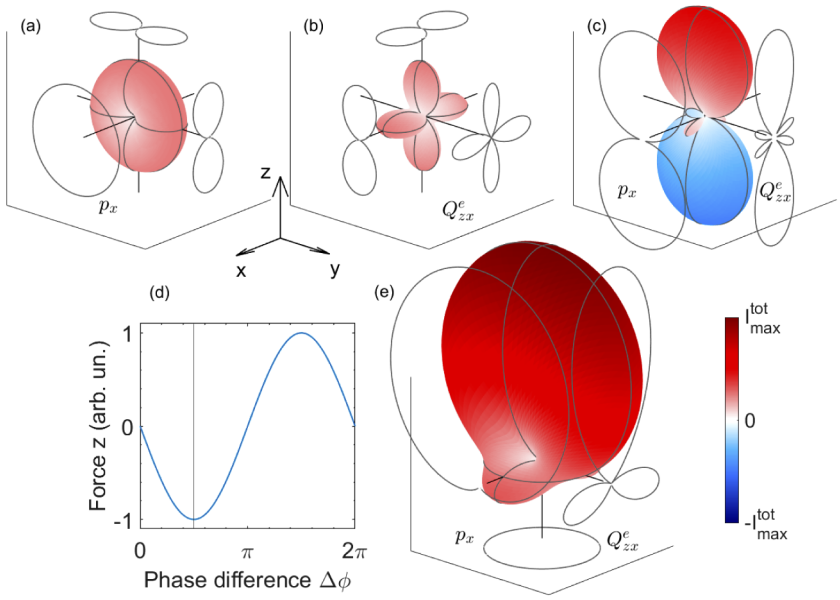

Fig. 2. Origin of the optical force resulting from the superposition of an electric dipole p_x with an electric quadrupole Q^e_{zx}, as a function of their relative phase difference $\Delta\phi$. (a) Radiation pattern for the electric dipole. (b) Radiation pattern for the electric quadrupole. (c) Interference pattern for $\Delta\phi = \pi/2$. (d) Normalized force dependency on the relative phase difference between both multipoles. (e) Total intensity distribution due to the sum of both multipoles. All patterns are normalized to the maximum intensity in panel (e). (Visualization 3) Intensity distribution for different values of the relative phase difference.

Optics EXPRESS

$\Delta\phi = \pi/2$. The full dependency of the total intensity and interference pattern on the phase difference can be found in Visualization 3. From the last paragraph in Sec. 3.1, it is clear that not all multipolar terms require a separate analysis, as soon as they can be obtained by rotations of other terms. For instance, we can skip the consideration of p_y and Q^e_{zy} by referring to the p_x and Q^e_{zx} interaction pattern.

Next, we consider the radiation pattern for the interaction of p_z and Q^e_{zz}, shown in Fig. 3 for the phase difference $\Delta\phi = \pi/2$, with the full dependency on the phase presented in Visualization 4.

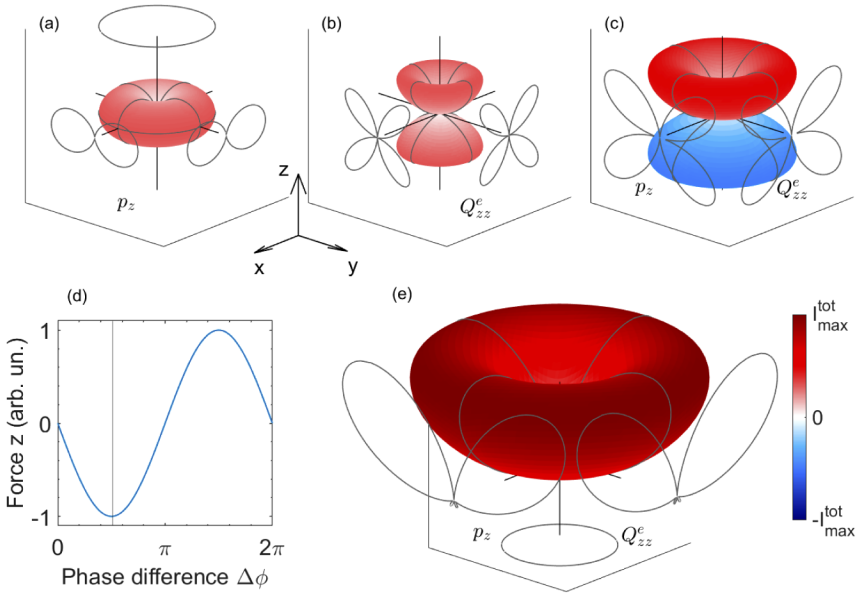

Fig. 3. Origin of the optical force resulting from the superposition of an electric dipole p_z with an electric quadrupole Q^e_{zz}, as a function of their relative phase difference $\Delta\phi$. (a) Radiation pattern for the electric dipole. (b) Radiation pattern for electric quadrupole. (c) Interference pattern for $\Delta\phi = \pi/2$. (d) Normalized force dependency on the relative phase difference between both multipoles. (e) Total intensity distribution due to the sum of both multipoles. All patterns are normalized to the maximum intensity in panel (e). (Visualization 4) Intensity distribution for different values of the relative phase difference.

The interaction of magnetic dipoles and quadrupoles is determined by the term

$$\langle \mathbf{F} \rangle_z = -\frac{k^5}{40\pi\varepsilon_0 c_0^2} \mathrm{Im}[Q^m_{zx} m_x^* + Q^m_{zy} m_y^* + Q^m_{zz} m_z^*], \tag{18}$$

which has the same overall far-field radiation properties in terms of intensity as its electric counterparts. Thus, the interaction between magnetic multipoles can be fully described by Fig. 2 and 3. No rotation is required to obtain the corresponding magnetic radiation patterns in that case since they are essentially identical. Starting from dipolar-quadrupolar interactions, the ability to shape radiation in particular direction is clearly observed and sets a fundamental basis for ultra-directional photonics [74].

3.3. *Quadrupole–quadrupole interaction*

The quadrupole – quadrupole interaction, which has the greatest number of terms to consider, can be fully described by only three visualizations. This stems from the fact that the diagonal

Optics EXPRESS

quadrupolar components are not independent because of the vanishing trace of the quadrupolar tensor [100], i.e.,

$$Q^e_{xx} + Q^e_{yy} + Q^e_{zz} = 0. \tag{19}$$

Overall, these remarks suggest that, without loss of generality, we can set $Q^{\mathrm{e}}_{\mathrm{zz}} = 0$ and consider that $Q^{\mathrm{e}}_{\mathrm{xx}} = -Q^{\mathrm{e}}_{\mathrm{yy}}$. The same considerations can be applied to the magnetic quadrupolar components. Indeed, adding nonzero $Q^{\mathrm{e}}_{\mathrm{zz}}$ or Q^m_{zz} would modify the total intensity distribution in such a way that additional terms will be symmetric with respect to the xy-plane and thus unable to produce the force along the z-axis, as seen from Eq. (14). Therefore, the components involving $Q^{\mathrm{e}}_{\mathrm{xx}}$ and $Q^{\mathrm{e}}_{\mathrm{yy}}$ read,

$$\langle \mathbf{F} \rangle_z = -\frac{k^6}{240\pi\varepsilon_0 c_0}\mathrm{Re}[Q^{\mathrm{e}}_{\mathrm{xx}}Q^{m*}_{\mathrm{xy}} - Q^{\mathrm{e}}_{yy}Q^{m*}_{\mathrm{xy}}] = -2\frac{k^6}{240\pi\varepsilon_0 c_0}\mathrm{Re}[Q^{\mathrm{e}}_{\mathrm{xx}}Q^{m*}_{\mathrm{xy}}]. \tag{20}$$

The corresponding radiation pattern for this type of interaction is presented in Fig. 4 for $\Delta\phi = 0$. The dependence of the force and total intensity on the phase can be found in Visualization 5.

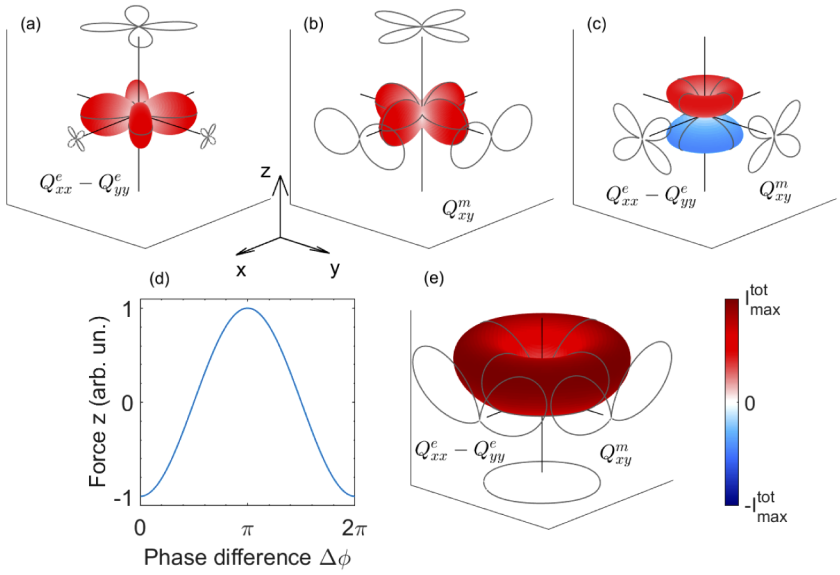

Fig. 4. Origin of the optical force resulting from the superposition of an electric quadrupole $Q^e_{xx} - Q^e_{yy}$ with a magnetic quadrupole Q^m_{xy}, as a function of their relative phase difference $\Delta\phi$. (a) Radiation pattern for the electric quadrupole. (b) Radiation pattern for the magnetic quadrupole. (c) Interference pattern for $\Delta\phi = 0$. (d) Normalized force dependency on the relative phase difference between multipoles. (e) Total intensity distribution due to the sum of both multipoles. All patterns are normalized to the maximum intensity in panel (e). (Visualization 5) Intensity distribution for different values of the relative phase difference.

The radiation pattern resulting from the Q^e_{zx} and Q^m_{zy} interaction is shown in Fig. 5 for a relative phase difference $\Delta\phi = 0$, with the full dependency on the phase presented in Visualization 6.

We can see that by increasing the orders of the interacting multipoles, more complicated radiation patterns appear, allowing higher directivity of the outgoing wave [72,73]. Remarkably, in all visualizations presented in this paper, the interference term conserves it shape and only scales depending on the amplitude and the relative phase difference between the multipoles.

Optics EXPRESS

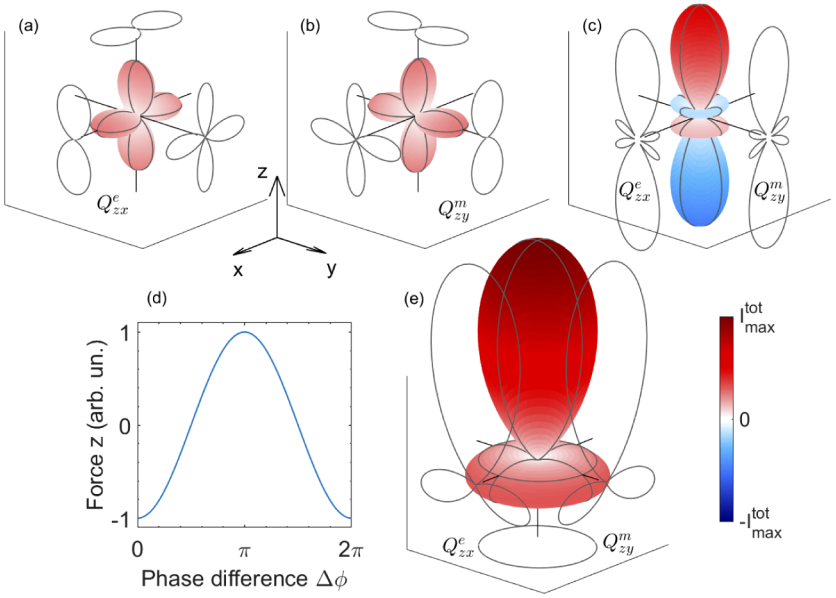

Fig. 5. Origin of the optical force resulting from the superposition of an electric quadrupole Q^e_{zx} with a magnetic quadrupole Q^m_{zy}, as a function of their relative phase difference $\Delta\phi$. (a) Radiation pattern for the electric quadrupole. (b) Radiation pattern for the magnetic quadrupole. (c) Interference pattern for $\Delta\phi = 0$. (d) Normalized force dependency on the relative phase difference between multipoles. (e) Total intensity distribution due to the sum of both multipoles. All patterns are normalized to the maximum intensity in panel (e). (Visualization 6) Intensity distribution for different values of the relative phase difference.

4. Conclusion and outlook

We have discussed the radiation from low-order multipoles interactions up to quadrupole – quadrupole interactions with the goal of explaining and illustrating the emergence of optical forces. The interference appearing as the result of the selected multipole interactions considered here has a very strong link with the optical force along a given direction of space and is effectively controlled by varying the relative amplitudes and phases between multipoles. The analytical considerations along with the visualizations provide a useful handle for particle manipulation analysis and for the development of ultra-directional scattering objects.

We also demonstrated that the total field intensity is not the only quantity, which determines the appearance of the force. Instead, it is the interference term between the multipoles that governs its emergence. We finally revealed that the shape of this interference term does not depend on the relative phase or relative amplitude of both multipoles; it can therefore serve as a reference metrics for the analysis of new and past experiments.

So far, the discussion has been carried out up to quadrupolar – quadrupolar interaction. Despite the fact that higher order multipoles will generally have less impact on the force for small isolated particles, they can find interesting applications in more advanced concepts, such as for example solar sails [101–103], where gratings or metasurfaces are utilized for light steering and higher order multipoles can be involved [104–106].

Overall, the approach developed in this paper facilitates the prediction and the analysis of the forces acting on micro and nanostructures illuminated by arbitrary light beams. The provided analysis can also stimulate the developments of an intuitive understanding of the forces at hand in near-field plasmonic experiments [6,107,108]. Based on the different interactions described

Optics EXPRESS

in this work, one can design optical structures that will support a given set of multimodes and, consequently, behave in a specific manner.

Funding

European Research Council (ERC-2015-AdG-695206); Schweizerischer Nationalfonds zur Förderung der Wissenschaftlichen Forschung (200020_153662).

Disclosures

The authors declare no conflicts of interest.

References

1. A. Ashkin, J. M. Dziedzic, J. E. Bjorkholm, and S. Chu, "Observation of a single-beam gradient force optical trap for dielectric particles," Opt. Lett. **11**(5), 288–290 (1986).
2. A. Ashkin, "Acceleration and Trapping of Particles by Radiation Pressure," Phys. Rev. Lett. **24**(4), 156–159 (1970).
3. W. D. Phillips, "Nobel Lecture: Laser cooling and trapping of neutral atoms," Rev. Mod. Phys. **70**(3), 721–741 (1998).
4. D. G. Grier, "A revolution in optical manipulation," Nature **424**(6950), 810–816 (2003).
5. J. R. Moffitt, Y. R. Chemla, S. B. Smith, and C. Bustamante, "Recent Advances in Optical Tweezers," Annu. Rev. Biochem. **77**(1), 205–228 (2008).
6. M. L. Juan, M. Righini, and R. Quidant, "Plasmon nano-optical tweezers," Nat. Photonics **5**(6), 349–356 (2011).
7. K. Dholakia and T. Čižmár, "Shaping the future of manipulation," Nat. Photonics **5**(6), 335–342 (2011).
8. S. E. S. Spesyvtseva and K. Dholakia, "Trapping in a Material World," ACS Photonics **3**(5), 719–736 (2016).
9. D. Gao, W. Ding, M. Nieto-Vesperinas, X. Ding, M. Rahman, T. Zhang, C. Lim, and C.-W. Qiu, "Optical manipulation from the microscale to the nanoscale: fundamentals, advances and prospects," Light: Sci. Appl. **6**(9), e17039 (2017).
10. A. F.-B. Itia, B. S. Alexander, K. S. Ethan, and R.-D. Halina, "Optical trapping in vivo: theory, practice, and applications," Nanophotonics **8**(6), 1023–1040 (2019).
11. A. Ashkin, J. M. Dziedzic, and T. Yamane, "Optical trapping and manipulation of single cells using infrared laser beams," Nature **330**(6150), 769–771 (1987).
12. K. Dholakia, M. MacDonald, and G. Spalding, "Optical tweezers: the next generation," Phys. World **15**(10), 31–35 (2002).
13. K. C. Neuman and S. M. Block, "Optical trapping," Rev. Sci. Instrum. **75**(9), 2787–2809 (2004).
14. M. Dienerowitz, M. Mazilu, and K. Dholakia, "Optical manipulation of nanoparticles: a review," J. Nanophotonics **2**(1), 021875 (2008).
15. N. Li, X.-M. Zhu, W.-Q. Li, Z.-H. Fu, M.-Z. Hu, and H.-Z. Hu, "Review of optical tweezers in vacuum," Front. Inf. Technol. Electron. Eng. **20**(5), 655–673 (2019).
16. W. Zhang, L. Huang, C. Santschi, and O. J. F. Martin, "Trapping and Sensing 10 nm Metal Nanoparticles Using Plasmonic Dipole Antennas," Nano Lett. **10**(3), 1006–1011 (2010).
17. M. Ploschner, M. Mazilu, T. Krauss, and K. Dholakia, "Optical forces near a nanoantenna," J. Nanophotonics **4**(1), 041570 (2010).
18. A. Lovera and O. J. F. Martin, "Plasmonic trapping with realistic dipole nanoantennas: Analysis of the detection limit," Appl. Phys. Lett. **99**(15), 151104 (2011).
19. C. Bradac, "Nanoscale Optical Trapping: A Review," Adv. Opt. Mater. **6**(12), 1800005 (2018).
20. S. Ghosh and A. Ghosh, "Next generation optical nanotweezers for dynamic manipulation: from surface to bulk," Langmuir **36**(21), 5691–5708 (2020).
21. A. S. Ang, A. Karabchevsky, I. V. Minin, O. V. Minin, S. V. Sukhov, and A. S. Shalin, "'Photonic Hook' based optomechanical nanoparticle manipulator," Sci. Rep. **8**(1), 2029 (2018).
22. L. Novotny and B. Hecht, *Principles of nano-optics* (Cambridge University, 2012).
23. J. Chen, J. Ng, K. Ding, K. H. Fung, Z. Lin, and C. T. Chan, "Negative Optical Torque," Sci. Rep. **4**(1), 6386 (2015).
24. D. Haefner, S. Sukhov, and A. Dogariu, "Conservative and Nonconservative Torques in Optical Binding," Phys. Rev. Lett. **103**(17), 173602 (2009).
25. L. Paterson, M. P. MacDonald, J. Arlt, W. Sibbett, P. E. Bryant, and K. Dholakia, "Controlled Rotation of Optically Trapped Microscopic Particles," Science **292**(5518), 912–914 (2001).
26. J. D. Jackson, *Classical electrodynamics* (John Wiley & Sons, 2007).
27. A. Salandrino, S. Fardad, and D. N. Christodoulides, "Generalized Mie theory of optical forces," J. Opt. Soc. Am. B **29**(4), 855–866 (2012).
28. J. Du, C.-H. Yuen, X. Li, K. Ding, G. Du, Z. Lin, C. T. Chan, and J. Ng, "Tailoring Optical Gradient Force and Optical Scattering and Absorption Force," Sci. Rep. **7**(1), 18042 (2017).
29. C. F. Bohren and D. R. Huffman, *Absorption and scattering of light by small particles* (John Wiley & Sons, 2008).
30. J. P. Gordon, "Radiation Forces and Momenta in Dielectric Media," Phys. Rev. A **8**(1), 14–21 (1973).

Optics EXPRESS

31. J. P. Barton, D. R. Alexander, and S. A. Schaub, "Theoretical determination of net radiation force and torque for a spherical particle illuminated by a focused laser beam," J. Appl. Phys. **66**(10), 4594–4602 (1989).
32. D. Richards, A. Zayats, M. Nieto-Vesperinas, P. C. Chaumet, and A. Rahmani, "Near-field photonic forces," Philos. Trans. R. Soc., A **362**(1817), 719–737 (2004).
33. R. E. Raab and O. L. De Lange, *Multipole theory in electromagnetism: classical, quantum, and symmetry aspects, with applications* (Oxford University, 2005).
34. J. Ng, C. T. Chan, P. Sheng, and Z. Lin, "Strong optical force induced by morphology-dependent resonances," Opt. Lett. **30**(15), 1956–1958 (2005).
35. J. Ng and C. T. Chan, "Size-selective optical forces for microspheres using evanescent wave excitation of whispering gallery modes," Appl. Phys. Lett. **92**(25), 251109 (2008).
36. J. Ng, R. Tang, and C. T. Chan, "Electrodynamics study of plasmonic bonding and antibonding forces in a bisphere," Phys. Rev. B **77**(19), 195407 (2008).
37. J. J. Xiao, J. Ng, Z. F. Lin, and C. T. Chan, "Whispering gallery mode enhanced optical force with resonant tunneling excitation in the Kretschmann geometry," Appl. Phys. Lett. **94**(1), 011102 (2009).
38. S.-H. Lee, Y. Roichman, and D. G. Grier, "Optical solenoid beams," Opt. Express **18**(7), 6988–6993 (2010).
39. J. Chen, J. Ng, Z. Lin, and C. T. Chan, "Optical pulling force," Nat. Photonics **5**(9), 531–534 (2011).
40. O. Brzobohatý, V. Karásek, M. Šiler, L. Chvátal, T. Čižmár, and P. Zemánek, "Experimental demonstration of optical transport, sorting and self-arrangement using a 'tractor beam'," Nat. Photonics **7**(2), 123–127 (2013).
41. S. Sukhov and A. Dogariu, "Negative Nonconservative Forces: Optical "Tractor Beams" for Arbitrary Objects," Phys. Rev. Lett. **107**(20), 203602 (2011).
42. A. Novitsky, C.-W. Qiu, and H. Wang, "Single Gradientless Light Beam Drags Particles as Tractor Beams," Phys. Rev. Lett. **107**(20), 203601 (2011).
43. K. Ding, J. Ng, L. Zhou, and C. T. Chan, "Realization of optical pulling forces using chirality," Phys. Rev. A **89**(6), 063825 (2014).
44. A. Dogariu, S. Sukhov, and J. Sáenz, "Optically induced 'negative forces'," Nat. Photonics **7**(1), 24–27 (2013).
45. A. S. Shalin, S. V. Sukhov, A. A. Bogdanov, P. A. Belov, and P. Ginzburg, "Optical pulling forces in hyperbolic metamaterials," Phys. Rev. A **91**(6), 063830 (2015).
46. K. Y. Bliokh and F. Nori, "Transverse and longitudinal angular momenta of light," Phys. Rep. **592**, 1–38 (2015).
47. H. Chen, Q. Ye, Y. Zhang, L. Shi, S. Liu, Z. Jian, and Z. Lin, "Reconfigurable lateral optical force achieved by selectively exciting plasmonic dark modes near Fano resonance," Phys. Rev. A **96**(2), 023809 (2017).
48. H. Chen, H. Zheng, W. Lu, S. Liu, J. Ng, and Z. Lin, "Lateral Optical Force due to the Breaking of Electric-Magnetic Symmetry," Phys. Rev. Lett. **125**(7), 073901 (2020).
49. F. J. Rodríguez-Fortuño, N. Engheta, A. Martínez, and A. V. Zayats, "Lateral forces on circularly polarizable particles near a surface," Nat. Commun. **6**(1), 8799 (2015).
50. K. Achouri, A. Kiselev, and O. J. F. Martin, "Multipolar origin of electromagnetic transverse force resulting from two-wave interference," Phys. Rev. B **102**(8), 085107 (2020).
51. M. Nieto-Vesperinas, J. J. Sáenz, R. Gómez-Medina, and L. Chantada, "Optical forces on small magnetodielectric particles," Opt. Express **18**(11), 11428–11443 (2010).
52. X. Xu, M. Nieto-Vesperinas, C.-W. Qiu, X. Liu, D. Gao, Y. Zhang, and B. Li, "Kerker-Type Intensity-Gradient Force of Light," Laser Photonics Rev. **14**(4), 1900265 (2020).
53. X. Xu and M. Nieto-Vesperinas, "Azimuthal Imaginary Poynting Momentum Density," Phys. Rev. Lett. **123**(23), 233902 (2019).
54. E. E. Radescu and G. Vaman, "Exact calculation of the angular momentum loss, recoil force, and radiation intensity for an arbitrary source in terms of electric, magnetic, and toroid multipoles," Phys. Rev. E **65**(4), 046609 (2002).
55. R. Alaee, C. Rockstuhl, and I. Fernandez-Corbaton, "Exact Multipolar Decompositions with Applications in Nanophotonics," Adv. Opt. Mater. **7**(1), 1800783 (2019).
56. R. Alaee, C. Rockstuhl, and I. Fernandez-Corbaton, "An electromagnetic multipole expansion beyond the long-wavelength approximation," Opt. Commun. **407**, 17–21 (2018).
57. W. Liu, A. E. Miroshnichenko, D. N. Neshev, and Y. S. Kivshar, "Broadband Unidirectional Scattering by Magneto-Electric Core–Shell Nanoparticles," ACS Nano **6**(6), 5489–5497 (2012).
58. B. Rolly, J.-M. Geffrin, R. Abdeddaim, B. Stout, and N. Bonod, "Controllable emission of a dipolar source coupled with a magneto-dielectric resonant subwavelength scatterer," Sci. Rep. **3**(1), 3063 (2013).
59. W. Liu, A. E. Miroshnichenko, R. F. Oulton, D. N. Neshev, O. Hess, and Y. S. Kivshar, "Scattering of core-shell nanowires with the interference of electric and magnetic resonances," Opt. Lett. **38**(14), 2621–2624 (2013).
60. W. Liu, J. Zhang, B. Lei, H. Ma, W. Xie, and H. Hu, "Ultra-directional forward scattering by individual core-shell nanoparticles," Opt. Express **22**(13), 16178–16187 (2014).
61. W. Liu, A. E. Miroshnichenko, and Y. S. Kivshar, "Control of light scattering by nanoparticles with optically-induced magnetic responses," Chin. Phys. B **23**(4), 047806 (2014).
62. J. Mäkitalo, M. Kauranen, and S. Suuriniemi, "Modes and resonances of plasmonic scatterers," Phys. Rev. B **89**(16), 165429 (2014).
63. A. I. Kuznetsov, A. E. Miroshnichenko, M. L. Brongersma, Y. S. Kivshar, and B. Luk'yanchuk, "Optically resonant dielectric nanostructures," Science **354**(6314), aag2472 (2016).

Optics EXPRESS

64. W. Liu and Y. S. Kivshar, "Multipolar interference effects in nanophotonics," Philos. Trans. R. Soc., A **375**(2090), 20160317 (2017).
65. Z.-J. Yang, R. Jiang, X. Zhuo, Y.-M. Xie, J. Wang, and H.-Q. Lin, "Dielectric nanoresonators for light manipulation," Phys. Rep. **701**, 1–50 (2017).
66. C. Yan, T. V. Raziman, and O. J. F. Martin, "Phase Bifurcation and Zero Reflection in Planar Plasmonic Metasurfaces," ACS Photonics **4**(4), 852–860 (2017).
67. C. Yan, K.-Y. Yang, and O. J. F. Martin, "Fano-resonance-assisted metasurface for color routing," Light: Sci. Appl. **6**(7), e17017 (2017).
68. H. K. Shamkhi, K. V. Baryshnikova, A. Sayanskiy, P. Kapitanova, P. D. Terekhov, P. Belov, A. Karabchevsky, A. B. Evlyukhin, Y. Kivshar, and A. S. Shalin, "Transverse Scattering and Generalized Kerker Effects in All-Dielectric Mie-Resonant Metaoptics," Phys. Rev. Lett. **122**(19), 193905 (2019).
69. A. B. Evlyukhin and B. N. Chichkov, "Multipole decompositions for directional light scattering," Phys. Rev. B **100**(12), 125415 (2019).
70. P. D. Terekhov, K. V. Baryshnikova, Y. A. Artemyev, A. Karabchevsky, A. S. Shalin, and A. B. Evlyukhin, "Multipolar response of nonspherical silicon nanoparticles in the visible and near-infrared spectral ranges," Phys. Rev. B **96**(3), 035443 (2017).
71. P. D. Terekhov, H. K. Shamkhi, E. A. Gurvitz, K. V. Baryshnikova, A. B. Evlyukhin, A. S. Shalin, and A. Karabchevsky, "Broadband forward scattering from dielectric cubic nanoantenna in lossless media," Opt. Express **27**(8), 10924–10935 (2019).
72. A. E. Krasnok, D. S. Filonov, C. R. Simovski, Y. S. Kivshar, and P. A. Belov, "Experimental demonstration of superdirective dielectric antenna," Appl. Phys. Lett. **104**(13), 133502 (2014).
73. A. E. Krasnok, C. R. Simovski, P. A. Belov, and Y. S. Kivshar, "Superdirective dielectric nanoantennas," Nanoscale **6**(13), 7354–7361 (2014).
74. A. I. Barreda, J. M. Saiz, F. González, F. Moreno, and P. Albella, "Recent advances in high refractive index dielectric nanoantennas: Basics and applications," AIP Adv. **9**(4), 040701 (2019).
75. R. R. Naraghi, S. Sukhov, and A. Dogariu, "Directional control of scattering by all-dielectric core-shell spheres," Opt. Lett. **40**(4), 585–588 (2015).
76. J. I. Dadap, J. Shan, and T. F. Heinz, "Theory of optical second-harmonic generation from a sphere of centrosymmetric material: small-particle limit," J. Opt. Soc. Am. B **21**(7), 1328–1347 (2004).
77. Y. Zhang, N. K. Grady, C. Ayala-Orozco, and N. J. Halas, "Three-Dimensional Nanostructures as Highly Efficient Generators of Second Harmonic Light," Nano Lett. **11**(12), 5519–5523 (2011).
78. V. K. Valev, X. Zheng, C. G. Biris, A. V. Silhanek, V. Volskiy, B. De Clercq, O. A. Aktsipetrov, M. Ameloot, N. C. Panoiu, G. A. E. Vandenbosch, and V. V. Moshchalkov, "The origin of second harmonic generation hotspots in chiral optical metamaterials [Invited]," Opt. Mater. Express **1**(1), 36–45 (2011).
79. M. Kauranen and A. V. Zayats, "Nonlinear plasmonics," Nat. Photonics **6**(11), 737–748 (2012).
80. S. D. Gennaro, M. Rahmani, V. Giannini, H. Aouani, T. P. H. Sidiropoulos, M. Navarro-Cía, S. A. Maier, and R. F. Oulton, "The Interplay of Symmetry and Scattering Phase in Second Harmonic Generation from Gold Nanoantennas," Nano Lett. **16**(8), 5278–5285 (2016).
81. J. Butet, G. D. Bernasconi, M. Petit, A. Bouhelier, C. Yan, O. J. F. Martin, B. Cluzel, and O. Demichel, "Revealing a Mode Interplay That Controls Second-Harmonic Radiation in Gold Nanoantennas," ACS Photonics **4**(11), 2923–2929 (2017).
82. G. Bautista, C. Dreser, X. Zang, D. P. Kern, M. Kauranen, and M. Fleischer, "Collective Effects in Second-Harmonic Generation from Plasmonic Oligomers," Nano Lett. **18**(4), 2571–2580 (2018).
83. A. Kiselev, G. D. Bernasconi, and O. J. F. Martin, "Modes interplay and dynamics in the second harmonic generation of plasmonic nanostructures," Opt. Express **27**(26), 38708–38720 (2019).
84. J. Butet, G. Bachelier, I. Russier-Antoine, C. Jonin, E. Benichou, and P. F. Brevet, "Interference between Selected Dipoles and Octupoles in the Optical Second-Harmonic Generation from Spherical Gold Nanoparticles," Phys. Rev. Lett. **105**(7), 077401 (2010).
85. T. Yamaguchi, Y. Okumura, and Y. Amemiya, "Wave impedance in the near field around the fundamental electromagnetic radiating elements," Electron. Comm. Jpn. Pt. I **74**(4), 86–95 (1991).
86. L. D. Landau and E. M. Lifshitz, *The Classical Theory of Fields* (Pergamon, 1971).
87. S. Nanz, *Toroidal Multipole Moments in Classical Electrodynamics: An Analysis of Their Emergence and Physical Significance* (Springer, 2016).
88. V. M. Dubovik and V. V. Tugushev, "Toroid moments in electrodynamics and solid-state physics," Phys. Rep. **187**(4), 145–202 (1990).
89. L. D. Barron, *Molecular light scattering and optical activity* (Cambridge University, 2009).
90. J. Applequist, "Traceless cartesian tensor forms for spherical harmonic functions: new theorems and applications to electrostatics of dielectric media," J. Phys. A: Math. Gen. **22**(20), 4303–4330 (1989).
91. X.-L. Zhang, S. B. Wang, Z. Lin, H.-B. Sun, and C. T. Chan, "Optical force on toroidal nanostructures: Toroidal dipole versus renormalized electric dipole," Phys. Rev. A **92**(4), 043804 (2015).
92. G. B. Arfken, H.-J. Weber, and F. E. Harris, *Mathematical Methods for Physicists: A Comprehensive Guide* (Academic, 2012).

Optics EXPRESS

93. A. Kiselev, K. Achouri, and O. J. F. Martin, "Matlab code for the visualization and force analysis of the electric and magnetic dipoles interference," (2020), https://doi.org/10.5281/zenodo.3891511.
94. J. M. Geffrin, B. García-Cámara, R. Gómez-Medina, P. Albella, L. S. Froufe-Pérez, C. Eyraud, A. Litman, R. Vaillon, F. González, M. Nieto-Vesperinas, J. J. Sáenz, and F. Moreno, "Magnetic and electric coherence in forward- and back-scattered electromagnetic waves by a single dielectric subwavelength sphere," Nat. Commun. **3**(1), 1171 (2012).
95. M. Kerker, D. S. Wang, and C. L. Giles, "Electromagnetic scattering by magnetic spheres," J. Opt. Soc. Am. **73**(6), 765–767 (1983).
96. A. V. Poshakinskiy and A. N. Poddubny, "Optomechanical Kerker Effect," Phys. Rev. X **9**(1), 011008 (2019).
97. B. García-Cámara, F. González, F. Moreno, and J. M. Saiz, "Exception for the zero-forward-scattering theory," J. Opt. Soc. Am. A **25**(11), 2875–2878 (2008).
98. W. Liu and Y. S. Kivshar, "Generalized Kerker effects in nanophotonics and meta-optics [Invited]," Opt. Express **26**(10), 13085–13105 (2018).
99. B. Rolly, B. Stout, and N. Bonod, "Boosting the directivity of optical antennas with magnetic and electric dipolar resonant particles," Opt. Express **20**(18), 20376–20386 (2012).
100. S. Mühlig, C. Menzel, C. Rockstuhl, and F. Lederer, "Multipole analysis of meta-atoms," Metamaterials **5**(2-3), 64–73 (2011).
101. L. Johnson, M. Whorton, A. Heaton, R. Pinson, G. Laue, and C. Adams, "NanoSail-D: A solar sail demonstration mission," Acta Astronaut. **68**(5-6), 571–575 (2011).
102. K. Achouri, O. V. Céspedes, and C. Caloz, "Solar "Meta-Sails" for Agile Optical Force Control," IEEE Trans. Antennas Propag. **67**(11), 6924–6934 (2019).
103. G. Swartzlander, L. Johnson, and B. Betts, "Light Sailing into the Great Beyond," Opt. Photonics News **31**(2), 30–37 (2020).
104. P. D. Terekhov, K. V. Baryshnikova, Y. Greenberg, Y. H. Fu, A. B. Evlyukhin, A. S. Shalin, and A. Karabchevsky, "Enhanced absorption in all-dielectric metasurfaces due to magnetic dipole excitation," Sci. Rep. **9**(1), 3438 (2019).
105. P. D. Terekhov, A. B. Evlyukhin, D. Redka, V. S. Volkov, A. S. Shalin, and A. Karabchevsky, "Magnetic Octupole Response of Dielectric Quadrumers," Laser Photonics Rev. **14**(4), 1900331 (2020).
106. E. A. Gurvitz, K. S. Ladutenko, P. A. Dergachev, A. B. Evlyukhin, A. E. Miroshnichenko, and A. S. Shalin, "The High-Order Toroidal Moments and Anapole States in All-Dielectric Photonics," Laser Photonics Rev. **13**(5), 1800266 (2019).
107. D. G. Kotsifaki and S. N. Chormaic, "Plasmonic optical tweezers based on nanostructures: fundamentals, advances and prospects," Nanophotonics **8**(7), 1227–1245 (2019).
108. A. Canós Valero, D. Kislov, E. A. Gurvitz, H. K. Shamkhi, A. A. Pavlov, D. Redka, S. Yankin, P. Zemánek, and A. S. Shalin, "Nanovortex-Driven All-Dielectric Optical Diffusion Boosting and Sorting Concept for Lab-on-a-Chip Platforms," Adv. Sci. **7**(11), 1903049 (2020).